Wettability evolution of different nanostructured cobalt films based on electrodeposition

Longlong Ju[1], *Han Xiao*[1], *Lei Ye*[1], *Anmin Hu*[2] ✉, *Ming Li*[1]

[1]*Shanghai Jiao Tong University, 800 Dongchuan Road, Shanghai 200240, People's Republic of China*
[2]*State Key Laboratory of Metal Matrix Composites, School of Materials Science and Engineering, Shanghai Jiao Tong University, 800 Dongchuan Road, Shanghai 200240, People's Republic of China*
✉ *E-mail: huanmin@sjtu.edu.cn*

Published in Micro & Nano Letters; Received on 21st January 2017; Revised on 3rd March 2017; Accepted on 9th March 2017

The wettability evolution of eight different types of nanostructured cobalt films is investigated using galvanostatic electrodeposition. The morphology, which evolves from a plump, pea-like structure to cone, pyramid, shell, fluffy cone, fluffy shell and flower structures can be controlled by changing the anion type in the electrolyte or the deposition current density. A growth mechanism is proposed based on cathodic anomalous absorption theory, which explains both the influence of the anion type on the surface structure and the current-dependent morphology evolution. The contact angle and sliding angle of all films are measured, and fractions of water drop contact area with the surrounding air are calculated to illustrate the roughness induced wettability. The hierarchical (nano and micro) structures exhibit eminent superhydrophobicity compared with single dimensional surfaces, indicating this as an effective way to prevent transition from Cassie–Baxter mode to Wenzel mode.

1. Introduction: Being an important transition metal, cobalt (Co) possesses favourable properties for catalysis [1, 2], solar energy absorption [3, 4] and magnetic recording [5]. These various properties are determined by the material's internal characters as well as the material morphology used, formed via different approaches or modified by tuning different synthetic parameters [6–8]. Therefore, how to control the synthesis of specific Co nanostructures has become an extremely valuable issue in functional materials fabrication.

At present, Co has a wide range of applications in aerospace, automotive, shipbuilding and other industries. Superhydrophobic Co performed self-cleaning, anti-corrosion, anti-ice and other superior properties, which make the industrial value of Co improved greatly. Superhydrophobicity of Co has become an important research topic in recent years [9]. Researchers have recently fabricated a variety of superhydrophobic Co nanostructures [10–14]. However, the growth mechanism of these superhydrophobic films was not discussed in detail in any of these cases. Generally, superhydrophobicity is a result of both low surface energy and rough morphology of a material, as explained by the Wenzel and Cassie models [15]. Although several researchers have proposed combinations of these two models [12], the relationship between Co film morphology, different models and wettability behaviour has not been discussed systematically. As such, it is worth studying the relationship between these models and wettability.

In this Letter, eight different types of Co nanostructures were fabricated by galvanostatic electrodeposition while controlling the electro-parameters in a simple and economical manner. Chemical modification was used to improve the superhydrophobicity. Contact angles (CAs) and sliding angles (SAs) were measured and area fractions were calculated to study the surface wettability. Wettability evolution of Co films was studied using different nanostructures.

2. Experiment: As reported by Hang *et al.* [16] and Wang *et al.* [17], Co nanostructured films were synthesised by both direct galvanostatic electrodeposition and a two-step plating method, using commercial pure (99.5%) copper (Cu) foils as base substrates. The Cu substrates were pretreated by electrochemical degreasing for 30 s, pickling liquor cleaning (10% H_2SO_4) for 20 s and deionised water cleaning for 30 s, and then dried in air. Different current densities and deposition times were employed to prepare samples with different nanostructures. The final products were observed and analysed by X-ray diffraction (XRD, Bruker D8 Discover) and scanning electronic microscopy (SEM, FEI, Sirion 200). The features on the products were approximately measured by the software attached to the SEM equipment.

The wettability of the Co nano-films was analysed at ambient temperature by a specific instrument (OCA20 dataphysics). Films were examined after immersion in stearic acid (ethanol) solution for 5 s to prepare low surface energy surfaces. Each CA or SA was measured repeatedly at different points, and the average of at least four measurements was reported in each case. CA and SA were compared and analysed under different models while the air fraction was also calculated to illustrate the roughness-induced superhydrophobicity.

3. Results and discussion: The transformation of surface microstructures was the main influential factor on the wettability evolution. This was first studied in different electrolyte to hydrochloric acid ratios, with solutions composed of the primary metal salt $CoCl_2{\cdot}6H_2O$ (100 g l^{-1}), an ammonium crystal modifier (100 g l^{-1}) and pH regulator buffer H_3BO_3 (35 g l^{-1}); the sulphuric system simply changed the main salt to $CoSO_4{\cdot}6H_2O$. After simple deposition at 1.25 – 12.5 Adm^{-2} for 2–20 min to prepare films with the same thickness, different types of nanostructured films were examined.

When $CoSO_4{\cdot}6H_2O$ was used as the main salt, bump shaped nanocrystals (herein type A) with average diameters of 600 nm formed (Fig. 1*a*), which were fabricated in the sulphuric system after deposition at 12.5 Adm^{-2} for 2 min. After deposition at 4 Adm^{-2} for 6.25 min, we obtained pea-shaped surfaces (type B) as shown in Fig. 1*b*, similar to elongated bumps. The CAs of these two nanostructured Co films were $124 \pm 2°$ and $144 \pm 2°$, respectively, both <150° and lower than the superhydrophobic standard. The CA of type B was larger than type A, due to the smaller size of the type B particles (300 nm average diameter) increasing the surface roughness more so than type A.

When other electrodeposition conditions fixed, the hydrochloric system under the same electrodeposition parameters yielded totally

doi: 10.1049/mnl.2017.0015

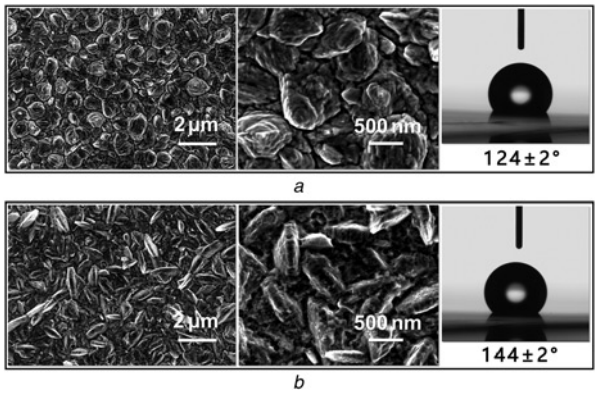

Fig. 1 *SEM images and CA of*
a Bump-shaped (type A) Co surfaces
b Pea-shaped (type B) Co surfaces

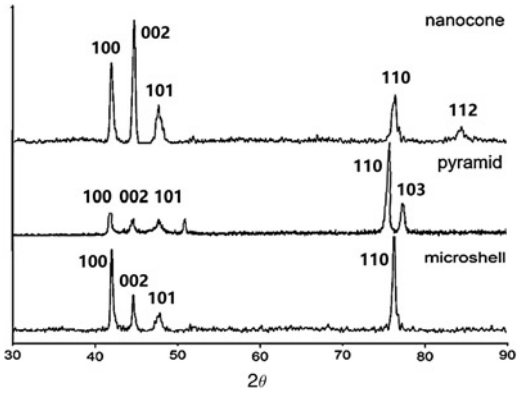

Fig. 3 *XRD patterns of types C, D and E surfaces*

different results compared with the sulphuric system. A higher current density (12.5 Adm^{-2} for 2 min) formed nanocones (type C), which were elongated triangular cones with an average length of ~250 nm at the bottom and an average height of ~500 nm (Fig. 2*a*). When the current was set to 4 Adm^{-2} and the time set to 6.25 min, the cones changed to pyramids (type D, Fig. 2*b*). The average edge length and height of pyramids increased to 600 and 800 nm, respectively. After the current density was decreased to 1.25 Adm^{-2} with 20 min deposition, the surface morphology changed to shell-like structures (type E), with 3 μm-long and 1 μm-high micro-shells (Fig. 2*c*). From a simple comparison of the surface morphologies, we can conclude that the electrolyte with chloride ion had a tendency to form sharp-edge crystallisation more so than sulphate ions, which can be explained using cathodic anomalous absorption (CAA) theory. Large cathodic ions such as sulphate, which has a high viscosity, tend to form wave-like features and interrupt the movement of cations to the anode. On the contrary, chloride ion is smaller, which has a lower viscosity, forming sharp features and promoting the movement of cations. Moreover, all CAs of types C, D and E are larger than 150°, indicating excellent superhydrophobicity behaviour (Fig. 2). This is due to the fact that the roughness values of the Co film surfaces were significantly higher in the hydrochloric system, making the actual contact area of the water droplets on the nanocones, pyramid and shell-like structures larger than in the bump or pea-like structures. We can therefore conclude that the sulphuric system is not suitable for the preparation of superhydrophobic Co films under the electrodeposited conditions in this research.

The chloride ion-based plated Co films have various morphologies depending on the current density and deposition time used in their creation. A proposed mechanism of dendritic growth is introduced to illustrate the different morphology outcomes under different current densities. A high current density promotes nucleation, generating dense and concentrated microstructures in fixed areas. Conversely, the amount of nucleation will decrease and the resulting crystals will be larger after deposition for longer times under lower current densities. The microstructure morphology is closely related to the growth direction of the crystal. XRD patterns of types C, D and E Co surfaces are shown in Fig. 3, which match well to standard Co diffraction peaks (JCP no. 05-0727). Meanwhile, for nanocones and microshells, the intensity of the (1 0 0) peak is obviously higher than for the pyramid surface,

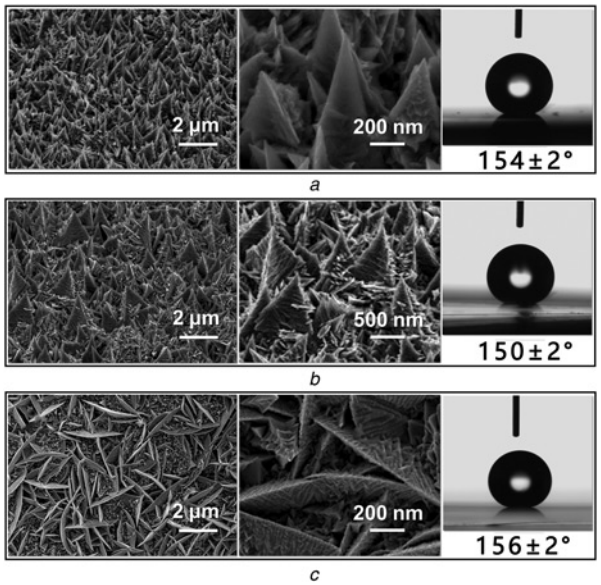

Fig. 2 *SEM images and CA of*
a Nanocones (type C) Co surfaces
b Shorter cones (pyramid-like, type D)
c Shell-structured (type E) Co surfaces

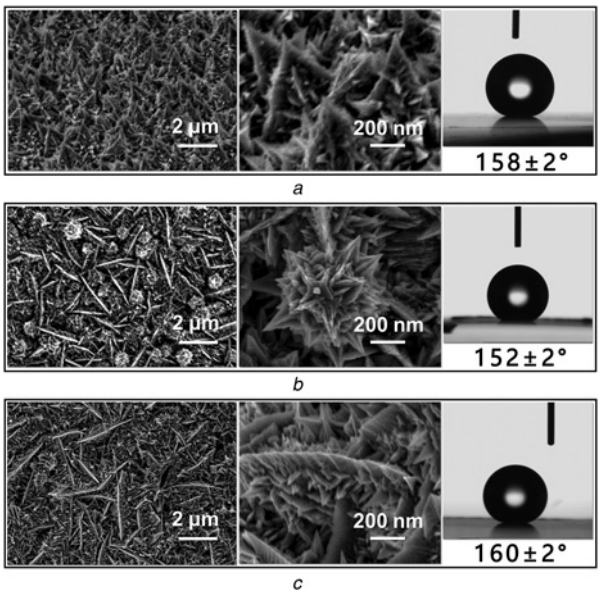

Fig. 4 *SEM images and CAs of hierarchical morphologies prepared by two-step method*
a Fluffy nanocones (type F) Co surfaces
b Floret-structured (type G) Co surfaces
c Fluffy shell-shaped (type H) Co surfaces

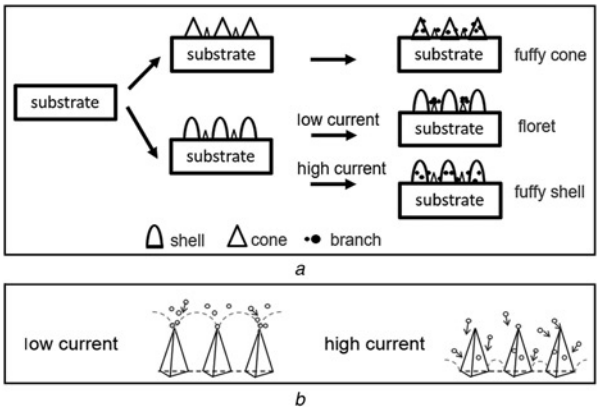

Fig. 5 *Schematic illustration of two-step method for hierarchical nanostructure growth and corresponding schematics of dendritic crystallisation*
a Schematic illustration of two-step method of hierarchical nanostructure growth
b Proposed corresponding schematics of dendritic crystallisation under different electro-parameters

suggesting more Co atoms along the (1 0 0) direction. Similarly, microshells grow strongly along the (1 1 0) direction as indicated by the highest (1 1 0) peak among the three curves, and nanocones grow most strongly along the (0 0 2) direction. However, the pyramid structure's XRD pattern shows lower intensity in both the (1 0 0) and (0 0 2) planes, and low intensity in (1 0 3) plane, indicating disorder along these two directions. This leads to a higher height of the pyramids than types C or E, enhancing the disorder of surfaces and making the CA slightly smaller than the other two structures.

Hierarchical structures were also obtained by two-step deposition; Fig. 4 shows a schematic illustration of this method for hierarchical nanostructure growth. First, nanocones or shell bases were fabricated under 12.5 Adm^{-2} for 2 min and 1.25 Adm^{-2} for 20 min, respectively. Then, the bases were branched by electrodeposition under different current densities. The crystal growth can be tuned at this stage by changing the current density. Fig. 4*a* shows SEM images of hierarchical nanocones grown in this manner. Many tiny nanocones were produced on the original nanocone surfaces under 4 Adm^{-2} for 6.25 min, forming fluffy nanocones (type F). The CA increased from $154 \pm 2°$ to $158 \pm 2°$, since more space was available for air cushions due to the hierarchical nanocones. Correspondingly, Figs. 4*b* and *c* show two-step deposited structures based on the shell-like film. When the second deposition employed a low current density, i.e. 4 Adm^{-2} for 6.25 min, floret-structured (type G) Co surfaces were fabricated. Scattered flower-like crystals 1 μm in diameter were formed between the shells. Under a higher current density of 12.5 Adm^{-2} for 2 min, fluffy shell-shaped (type H) Co films were formed with very tiny nanocones on the two sides of the shells. Compared with type E, the fluffy structure is more hydrophobic (CA increases to $160 \pm 2°$), due to its hierarchical structure that intensifies the air cushioning effect. Meanwhile, the flower structures are unequally scattered and peaked over the base, discouraging bubble formation and reducing the CA to $152 \pm 2°$.

A schematic illustration of this two-step method for hierarchical nanostructure growth is shown in Fig. 5*a*, along with the proposed corresponding schematics of dendritic crystallisation under different electrodeposition parameters (Fig. 5*b*). If the current density is relatively lower, the metal cations are prone to depositing on the small cone tips among the shells, gradually forming discrete flowers between the valleys in accordance with the metal-ion deficient layer theory [17]. Under low current, Co atoms tend to flow to the tip of the shells and leave a dip between each nucleus, forming floret structure. However, when the current density is higher by a certain amount, the nucleus would also grow on the flat surfaces similar to the two sides of the micro-shells, fabricating fluffy hierarchical nanostructures. This is because the speed of atomic deposition is faster under a higher current density. For Co atoms, the time of nucleation is too short to move to the theoretical growth position.

Based on the CAs and SAs shown in Table 1, the nanocones, pyramids, shells, floret, fluffy cones and fluffy shells (types C, D, E, F, G and H) exhibit superhydrophobic behaviour (water CA > 150°). Meanwhile the bump, pea-like structures and corns are water adhesive (SA > 90°). For the bump and pea structures, the relatively smooth surfaces may have lower SA and thus are neither Wenzel nor Cassie mode surfaces. For the cones, the sharp tips and the grooves increased the roughness of the surface, leading to pinning of water. The rougher morphology exhibits high superhydrophobicity, and the water drop does not roll down the surface even after being oriented vertically, indicating Wenzel mode. The CA and SA for type D (pyramids), E (shells) and hierarchical structure F (fluffy cones), G (floret) and H (fluffy shells) are 150°, 156°, 158°, 152°, 160° and 23°, 10°, 7°, 18°, 4°, respectively. These five types are in Cassie mode. A large number of tiny nanocones distributed on the surface irregularly, making structures of these five types more complex. The droplet is prevented to touch the surface because more air pockets are held, as a result of which, perfect superhydrophobic surfaces in Cassie mode form. We can calculate the area fraction using Cassie's law as follows [18]

$$\cos\theta_c = f_{sl}(\cos\theta_{sl} + 1) - 1 \quad (1)$$

Here θ_c is the CA of different structures (Table 1), θ_{sl} is the CA of a smooth surface (83°) [10] and f_{sl} is the area fractions of the touched interface between liquid and solid. Therefore, air fractures on the types D, E, F, G and H surfaces are calculated as 0.119, 0.077, 0.065, 0.104 and 0.054, which are extremely low (Table 1). In fact, the pyramid and shell-like structures can be considered as one-step products that have simple hierarchical construction. In all, this may provide a way to better control the structure hierarchy and realise transitions from Wenzel mode to Cassie mode.

4. Conclusion: Wettability evolution of Co films is dependent on the surface nanostructures, which can be controlled by differing the electro-parameters such as electrolyte composition, current density, time and the number of deposition steps. Electrolytes with chloride ion have a tendency to undergo sharper edge crystallisation compared with sulphate ion systems based on CAA theory. The chloride ion-based plated Co films have various morphologies under different current densities and deposition times. Single crystalline surfaces of both Co shell structures and cone structures grow along certain directions, yielding better superhydrophobic performance than Co pyramid structures. A proposed mechanism of two-step dendritic growth was introduced to illustrate the

Table 1 Measured CA, SA (±2°) and calculated area fraction of the eight different types of Co surfaces, respectively

Type no.	A	B	C	D	E	F	G	H
CA, deg	124	144	154	150	156	158	152	160
SA, deg	>90	>90	>90	23	10	7	18	4
area fraction	–	–	–	0.119	0.077	0.065	0.104	0.054

doi: 10.1049/mnl.2017.0015

morphology outcomes under different current densities. Among the eight different nanostructured films, the hierarchical (fluffy shell) structures exhibited eminent superhydrophobicity and non-sticky properties compared with single-dimensional surfaces, indicating an effective way to prevent transitions from Cassie–Baxter mode to Wenzel mode in such systems.

5. Acknowledgments: This work was sponsored by National Natural Science foundation of China (grant no. 61176097) and (grant no. 61376107). The authors thank the Instrumental Analysis Center of Shanghai Jiao Tong University, for the use of the SEM equipment.

6 References

[1] Cobo S., Heidkamp J., Jacques P.A., *ET AL.*: 'A janus cobalt-based catalytic material for electro-splitting of water', *Nat. Mater.*, 2012, **11**, (9), pp. 802–807

[2] Yang J., Bao C., Zhu K., *ET AL.*: 'High catalytic activity and stability of nickel sulfide and cobalt sulfide hierarchical nanospheres on the counter electrodes for dye-sensitized solar cells', *Chem. Commun. (Camb.)*, 2014, **50**, (37), pp. 4824–4826

[3] Shukla S., Loc N.H., Boix P.P., *ET AL.*: 'Iron pyrite thin film counter electrodes for dye-sensitized solar cells: high efficiency for iodine and cobalt redox electrolyte cells', *ACS Nano*, 2014, **8**, (10), pp. 10597–10605

[4] Huo J., Zheng M., Tu Y., *ET AL.*: 'A high performance cobalt sulfide counter electrode for dye-sensitized solar cells', *Electrochim. Acta*, 2015, **159**, pp. 166–173

[5] Wu L., Jubert P.O., Berman D., *ET AL.*: 'Monolayer assembly of ferrimagnetic Co(X)Fe(3-X)O4 nanocubes for magnetic recording', *Nano. Lett.*, 2014, **14**, (6), pp. 3395–3399

[6] An Z.-g., Zhang J.-j., Pan S.-l.: 'Simple synthesis and characterization of highly ordered sisal-like cobalt superstructures', *Mater. Chem. Phys.*, 2010, **123**, (2–3), pp. 795–800

[7] Li H., Jin Z., Song H., *ET AL.*: 'Synthesis of Co submicrospheres self-assembled by Co nanosheets via a complexant-assisted hydrothermal approach', *J. Magn. Magn. Mater.*, 2010, **322**, (1), pp. 30–35

[8] Cheng G.: 'Facile synthesis of leaf-like cobalt microstructures at low temperature', *Micro Nano Lett.*, 2014, **9**, (5), pp. 312–314

[9] Lin Feng S.h.L., Li Y., Li H., *ET AL.*: 'Super-hydrophobic surfaces: from natural to artificial', *Adv. Mater.*, 2002, **14**, (24), pp. 1857–1860

[10] Qiu R., Wang P., Zhang D., *ET AL.*: 'One-step preparation of hierarchical cobalt structure with inborn superhydrophobic effect', *Colloids Surf. A, Physicochem. Eng. Asp.*, 2011, **377**, (1–3), pp. 144–149

[11] Basu B.J., Manasa J.: 'Reversible switching of nanostructured cobalt hydroxide films from superhydrophobic to superhydrophilic state', *Appl. Phys. A*, 2011, **103**, (2), pp. 343–348

[12] Xiao H., Hu A., Hang T., *ET AL.*: 'Electrodeposited nanostructured cobalt film and its dual modulation of both superhydrophobic property and adhesiveness', *Appl. Surf. Sci.*, 2015, **324**, pp. 319–323

[13] Jiang X., Hu W., Peng C., *ET AL.*: 'Simultaneous fabrication of superhydrophobic cathodic cobalt and anodic copper surfaces by a one-step electrodeposition process', *Mater. Res. Innov.*, 2015, **19**, (sup2), pp. S2-83–S82-89

[14] Belov A.S., Zelinskii G.E., Varzatskii O.A., *ET AL.*: 'Molecular design of cage Iron(Ii) and Cobalt(Ii,Iii) complexes with a second fluorine-enriched superhydrophobic shell', *Dalton Trans.*, 2015, **44**, (8), pp. 3773–3784

[15] Darmanin T., de Givenchy E.T., Amigoni S., *ET AL.*: 'Superhydrophobic surfaces by electrochemical processes', *Adv. Mater.*, 2013, **25**, (10), pp. 1378–1394

[16] Hang T., Hu A., Li M., *ET AL.*: 'Structural control of a cobalt nanocone array grown by directional electrodeposition', *CrystEngComm*, 2010, **12**, (10), p. 2799

[17] Wang H., Hu A., Li M.: 'Synthesis of hierarchical mushroom-like cobalt nanostructures based on one-step galvanostatic electrochemical deposition', *CrystEngComm*, 2014, **16**, (34), p. 8015

[18] Cassie A.B.D.: 'Wettability of porous surfaces', *Trans. Faraday Soc.*, 1944, **40**, pp. 546–551